

## Ultra-fast pg/ml anthrax toxin (protective antigen) detection assay based on microwave-accelerated metal-enhanced fluorescence

Anatoliy I. Dragan<sup>a</sup>, Mark T. Albrecht<sup>b</sup>, Radmila Pavlovic<sup>a</sup>, Andrea M. Keane-Myers<sup>b</sup>, Chris D. Geddes<sup>a,\*</sup>

<sup>a</sup> Institute of Fluorescence, University of Maryland, Baltimore County, Baltimore, MD 21202, USA

<sup>b</sup> Biological Defense Research Directorate, Naval Medical Research Center, Silver Spring, MD 20910, USA

### ARTICLE INFO

#### Article history:

Received 12 December 2011  
Received in revised form 28 February 2012  
Accepted 29 February 2012  
Available online 6 March 2012

#### Keywords:

Metal-enhanced fluorescence  
Surface-enhanced fluorescence  
Plasmon-enhanced fluorescence  
Plasmon-controlled fluorescence  
Point-of care diagnostics  
Anthrax  
Protective antigen (PA)  
Pathogen detection  
Bio-warfare agent detection

### ABSTRACT

Rapid presymptomatic diagnosis of *Bacillus anthracis* at early stages of infection plays a crucial role in prompt medical intervention to prevent rapid disease progression and accumulation of lethal levels of toxin. To detect low levels of the anthrax protective antigen (PA) exotoxin in biological fluids, we have developed a metal-enhanced fluorescence (MEF)–PA assay using a combination of the MEF effect and microwave-accelerated PA protein surface absorption. The assay is based on a modified version of our “rapid catch and signal” (RCS) technology previously designed for the ultra-fast and sensitive analysis of genomic DNA sequences. Technologically, the proposed MEF–PA assay uses standard 96-well plastic plates modified with silver island films (SiFs) grown within the wells. It is shown that the fluorescent probe, covalently attached to the secondary antibody, plays a crucial role of indicating complex formation (i.e., shows a strong MEF response to the recognition event). Microwave irradiation rapidly accelerates PA deposition onto the surface (“rapid catch”), significantly speeding up the MEF–PA assay and resulting in a total assay run time of less than 40 min with an analytical sensitivity of less than 1 pg/ml PA.

© 2012 Elsevier Inc. All rights reserved.

Bacterial infection typically alters the host's homeostasis triggering perturbations to various cellular and molecular networks. Biomarkers indicative of this altered condition can be either pathogen- or host-derived. Common targets include measurable genes, proteins, metabolites, and other indicators associated with immunological, pathological, and/or clinical outcomes [1]. Rapid detection of these biomarkers at early stages of infection increases the chances of an accurate diagnosis when the patient is presymptomatic, and successful medical intervention can be initiated. This is particularly critical for the treatment of *Bacillus anthracis*, the etiological bacterium of anthrax, which is often difficult to diagnose and spreads rapidly in the patient.

Clinically, anthrax presents with three different pathologies depending on the route of infection. These are cutaneous anthrax, typically identified by the appearance of a black eschar on the skin at the site of infection [2], gastrointestinal anthrax, which resembles generic food poisoning [3], and inhalational anthrax. Inhalational is the most serious form of anthrax infection and

initially presents with a nonspecific prodrome resembling the flu followed by severe respiratory distress, septic shock, and death [4]. Unfortunately, other conditions present with similar symptoms, confounding an obvious diagnosis [3]. The ability of *B. anthracis* to form an environmentally hardened spore allows for aerosolized dispersion and has prompted its use as a bioterrorism agent [5]. Inhalation of aerosolized spores results in a high percentage of morbidity and mortality due to the high exposure and infection potential. If diagnosis and proper medical intervention are not initiated early enough, the infection rapidly progresses to a point where antibiotic therapy is no longer effective due to the accumulation of lethal levels of toxin [6,7]. At this stage of the infection, the prognosis is poor; even with therapeutic intervention, inhalational anthrax has a mortality rate between 60 and 100% [5,8,9].

Inhalational anthrax involves a complex series of host–pathogen interactions. The majority of the inhaled endospores are immediately ingested by pulmonary phagocytes and subsequently transported to the bloodstream through the lymphatic channels to the hilar and tracheobronchial lymph nodes [10–13]. During trafficking to these regional lymph nodes through the bloodstream, the endospores begin the germination process, resulting in the production of two exotoxins composed of binary combinations

\* Corresponding author. Fax: +1 410 576 5722.

E-mail address: [geddes@umbc.edu](mailto:geddes@umbc.edu) (C.D. Geddes).

of protective antigen (PA)<sup>1</sup> and either lethal factor (LF) or edema factor (EF) [14]. These toxin proteins are analogous to other AB-type toxins and form lethal toxin (LT), from the combination of LF and PA, and/or edema toxin (ET), from the combination of EF and PA. Binding to PA occurs on the cell surface after cleavage and activation of full-length PA to PA63 by furin [14,15]. The activated PA63 conformer oligomerizes to form a heptamer that binds up to three molecules of LF, EF, or a mixture of the two [16,17]. The central role of PA during the intoxication process is further highlighted by its messenger RNA (mRNA) expression levels, which are reported to be 4-fold higher than LF and 14-fold higher than EF [18]. Following endocytosis of the toxin complex and subsequent acidification of the endosome, the PA63 heptamer inserts into the membrane, forming a channel through which LF and EF enter the cytosol [19]. Both toxins serve to disable the immune system. LF, a zinc-dependent endopeptidase, specifically cleaves mitogen-activated protein kinases down-regulating both innate and acquired immune responses, whereas EF, an adenylate cyclase, incapacitates phagocytes and causes edema through cyclic AMP induction and accumulation of fluid [20]. The prominence of the PA fraction of the anthrax tripartite toxin and its elevated expression levels relative to the other toxin components during pathogenesis make it an ideal biomarker for diagnostic detection.

Traditional diagnosis of anthrax uses the patient's history and a battery of tests that evaluate standard morphological and phenotypic properties. These procedures involve culturing blood or cerebrospinal fluid overnight, followed by multiple hours of biochemical testing and microscopy [21]. Although definitive, the isolation of *B. anthracis* from biological samples is possible only late in the disease process [22]. Serological diagnosis is also an accepted technique that is sensitive and specific, but antibody responses to *B. anthracis* require between 8 and 12 days to develop [23]. Attempts to maintain sensitivity while reducing the time between sample collection and diagnosis have resulted in numerous genotypic identification methods using polymerase chain reaction (PCR) or reverse transcription (RT)-PCR amplification to detect anthrax-specific DNA or mRNA sequences, respectively [3]. Identification of *B. anthracis* infection has also been demonstrated with various immunoassays directed against key biomarkers that characterize anthrax, including spore coat antigens and toxins. These approaches are dependent on target acquisition and identification through the interaction of multiple antibodies and a chromogenic substrate [24–26]. Unfortunately, the requirement of a chromogenic substrate limits both biomarker resolution and the detection limit (to ~1 ng/ml). For instance, sandwich enzyme-linked immunosorbent assays (ELISAs) developed for the detection of anthrax PA exotoxin using monoclonal and polyclonal antibodies achieve the same lower PA detection limit of approximately 1 ng/ml for a detection time of more than 4 to 5 h [25,27]. Development of fluorescence-based assays with increased sensitivity, such as immunoassay using europium nanoparticles (NPs) [26], fluorescent covalent microspheres [28], and fluorescence resonance energy transfer (FRET) assay [29], have protein sensitivity in a range from 10 pg/ml to 60 ng/ml and an assay PA detection time of more than 4 to 5 h. Recently reported approaches for anthrax protein toxins, such as assays based on multiwall carbon nanotube sensors [30]

and on matrix-assisted laser desorption/ionization time-of-flight (MALDI-TOF) mass spectrometry [31], have relatively higher detection limits of 30 ng/ml and 5 pg/ml, respectively, whereas detection time, especially for the MALDI-TOF assay, is long and includes an overnight incubation stage. In essence, currently known anthrax toxin assays have a broad range of sensitivities and require multiple time-consuming incubations.

The goal of this study was to develop a PA detection assay that is both rapid (<1 h) and ultra-sensitive (~pg/ml). These requirements regarding the detection time and sensitivity of the assay are critically important for early diagnosis of the disease and its successful care.

Direct detection of toxin in biological fluids following its production is an ideal approach to diagnosis because it avoids extended incubations associated with culturing and amplification. Recent advances in the field of fluorescence spectroscopy have yielded a new platform technology for fluorescence surface bioassays called microwave-accelerated metal-enhanced fluorescence (MAMEF). This technique reliably detects proteins [32–34] and nucleic acids [35–37] at nanogram levels and below from biological fluids within seconds. This ultra-fast technology is based on metal-enhanced fluorescence (MEF), a phenomenon that dramatically enhances chromophores' emission when in close proximity to silver NPs [38,39]. MEF is based on the specific coupling of both the ground and excited state fluorophores with the surface plasmon electrons of the proximal silver NPs, resulting in enhancement of emission and typically reducing the excited state lifetime [38,39].

Another component of the MAMEF technology is the use of low-power microwave irradiation of samples, which increases the rate of mass transportation and molecular diffusion, resulting in an increase in the analyte detection limit [40,41]. Adaptation of this sensitive, low-cost, and ultra-fast technique to the detection of PA during presymptomatic *B. anthracis* infection may well eliminate the need for multiple diagnostic tests and enable early therapeutic intervention.

In this article, we describe and characterize a novel MAMEF-PA assay that was designed especially for the detection of low levels of anthrax exotoxin, PA, in solution.

## Materials and methods

Silver nitrate (99.9%), sodium hydroxide (99.996%), ammonium hydroxide (30%), and D-glucose were purchased from Sigma-Aldrich (USA). Immulon 4 HBX 1 × 12 Strip flat-bottom plates were purchased from Thermo Scientific (USA).

Recombinant full-length PA (PA83) protein, primary antibody for PA (IQNPA anti-PA), was supplied by IQ Corporation (Netherlands) and has been described previously [42]. Secondary antibody, fluorescein isothiocyanate (FITC) Pierce Rabbit Anti-Human Immunoglobulin G (IgG, FC fragment specific, fluorescein conjugated), was purchased from Thermo Scientific.

Milk Diluent/Blocking solution was purchased from KPL (USA). SuperBlock blocking buffer in phosphate-buffered saline (PBS) was obtained from Thermo Scientific.

### Preparation of SiFs

Preparation of silver island films (SiFs) on the bottom of Immulon 4 HBX plate wells was undertaken using a modified protocol as described previously [40]. This includes the preparation of a silvering solution. Here 200 µl of sodium hydroxide solution (0.5%, w/v) is added to 60 ml of AgNO<sub>3</sub> (0.83%, w/v) and the solution becomes brown and cloudy, after which 2 ml of ammonium hydroxide (30% solution) is added until the solution becomes clear. The solution is

<sup>1</sup> Abbreviations used: PA, protective antigen; LF, lethal factor; EF, edema factor; LT, lethal toxin; ET, edema toxin; mRNA, messenger RNA; PCR, polymerase chain reaction; RT, reverse transcription; ELISA, enzyme-linked immunosorbent assay; NP, nanoparticle; FRET, fluorescence resonance energy transfer; MALDI-TOF, matrix-assisted laser desorption/ionization time-of-flight; MAMEF, microwave-accelerated metal-enhanced fluorescence; MEF, metal-enhanced fluorescence; FITC, fluorescein isothiocyanate; IgG, immunoglobulin G; SiF, silver island film; DT, deposition time; OD, optical density; CCD, charge-coupled device; 1°, primary antibody; 2°, secondary antibody; St-F, streptavidin-FITC; FDTD, finite difference time domain; MW, microwave irradiation; LoD, limit of detection; LLoQ, lower limit of quantitation.

then cooled down on ice to 10 °C, and 15 ml of fresh D-glucose solution (4.8%, w/v) is added while stirring.

The silvering solution is then loaded into preheated (40 °C) plate wells for 2 min, followed by cooling on ice for 4 min. The plate is then placed on a heater (40 °C) for different deposition times (DTs) from 2 to 12 min. The plate is then washed several times with deionized water and dried with a stream of nitrogen gas.

The optical density (OD) spectra (absorption spectra) of SiF plates were measured using a Cary 50 Bio UV–VIS (ultraviolet–visible) Spectrophotometer equipped with a 50 MPR Microplate Reader (Varian).

#### Measurements of fluorescence

Fluorescence measurements of the fluorescein-labeled antibody in plate wells as well as excitation of emission were made by using a coupled fiber system (Fig. 1) attached to a Fiber Optic CCD (charge-coupled device) Spectrometer (HD2000) from Ocean Optics (USA). Excitation was undertaken using a 473-nm CW laser line. Notch and LongPass RazorEdge filters (Semrock, USA) were used to cut off the excitation light in the detection channel and to maximize the detection signal.

#### Attachment of PA to silver-coated Immulon 4 HBX plates

PA at different concentrations was dissolved in 1:20 (v/v) diluted milk diluent/blocking solution. Attachment of the PA protein to SiF plate wells was performed by incubation of PA solution (80 µl/well) at ambient temperature for 30 min or by microwave irradiation for different times (5–30 s) in a microwave cavity using a GE Compact Microwave (model JES735BF, frequency = 2.45 GHz, power = 700 W). The microwave irradiation power was reduced to 20%, which corresponded to 140 W over the entire cavity. After incubation (microwave irradiation), plate wells were washed extensively with deionized water and filled with buffer.

#### Formation of antibodies/PA complex

In this study, we used two protocols for the antibody attachment to PA.

##### Protocol 1

Protocol 1 is a commonly used procedure for standard ELISAs and approaches. It includes the following steps: add the PA sample into plate wells and incubating for 60 min; wash the wells to remove unattached protein; block the unoccupied surface with bovine serum albumin (BSA); add the primary antibody (1°), [anti-PA] = 50 nM, and incubate for 15 min; the 1° binds to PA; wash to remove unattached 1°; add secondary antibody (2°), [mouse anti-human IgG–biotin] = 50 nM, and incubate for 15 min; the 2° antibody attaches to 1°; wash to remove unattached 2°; add streptavidin–FITC (St–F), [St–F] = 50 nM, and incubate for 15 min; the St–F binds to biotin–2 complex; wash to remove unattached streptavidin; fill wells with buffer.

##### Protocol 2

Protocol 2 is a modification of the first protocol and was designed specifically to be much more rapid by reducing the total number of steps (reagents) used for antibody binding and “visualization” of PA on the surface. After incubating PA/milk (Milk Diluent/Blocking solution) in the wells as in protocol 1, the surface was rapidly blocked with SuperBlock solution without incubation; that is, after loading SuperBlock solution into wells, it was immediately removed and the wells were refilled. The procedure was repeated three times. Instead of using the streptavidin–biotin system in this

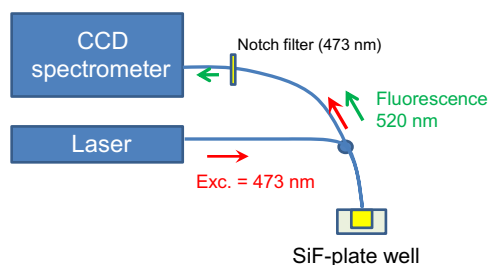


**Fig. 1.** Experimental setup for the MEF–PA assay. A bitruncated fiber was used both to deliver the excitation light to the sample and to collect the fluorescence, which after passing through a Notch filter to remove the 473-nm laser light falls incident on a CCD spectrometer.

protocol, we used a fluorescein-labeled secondary antibody. This omission removes one incubation/washing step, thereby speeding up the process. Binding of antibodies to the PA on the plate wells’ surface was performed by adding 80 µl of the milk solution containing a 1:1 (mol/mol) preformed complex of the primary and secondary antibodies (concentration of antibodies = 50 nM). Plates were incubated at ambient temperature for 30 min.

#### FDTD numerical simulations

The two-dimensional finite difference time domain (FDTD) simulations were used to simulate the effect of NP density, which increases during wet deposition of silver on glass slides, with the favorable effect of increasing the electric field intensity between the NPs.

For the simulations, the incident far field was defined as a plane wave with a wave vector that is normal to the injection surface, and the scattered and total fields were monitored during the simulation such that the total or scattered transmission could be measured. The excitation light (473 nm) was incident on the 200-nm silver NPs from the bottom along the y axis. Two NPs were attached to the glass slide. The distance between two silver NPs was systematically changed from 70 to 10 nm. Using FDTD Solutions software (Lumerical, Canada), the simulation region was set to 600 × 600 nm<sup>2</sup> with high mesh accuracy. To minimize simulation times and maximize the resolution of visualizing field enhancement around the metal particles, a mesh override region was set to 0.1 nm. The overall simulation time was set to 100 fs.

## Results and discussion

#### Physical characterization of SiF plates

Fig. 2 shows photographs of the original and silver-modified Immulon 4 HBX plates. The silver DT within wells was progressively increased from 0 to 12 min by row but remains constant

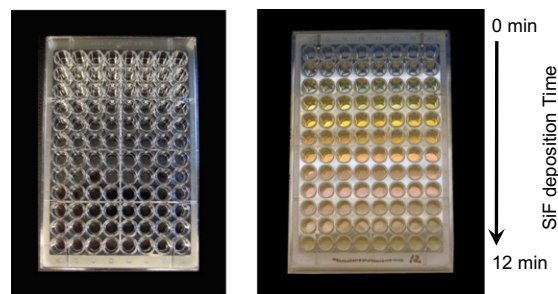


**Fig. 2.** Photographs of the original Immulon 4 HBX plate (left) and a silvered plate (SiF plate) (right). The silver DT was varied from 0 to 12 min (from the plate top to bottom).

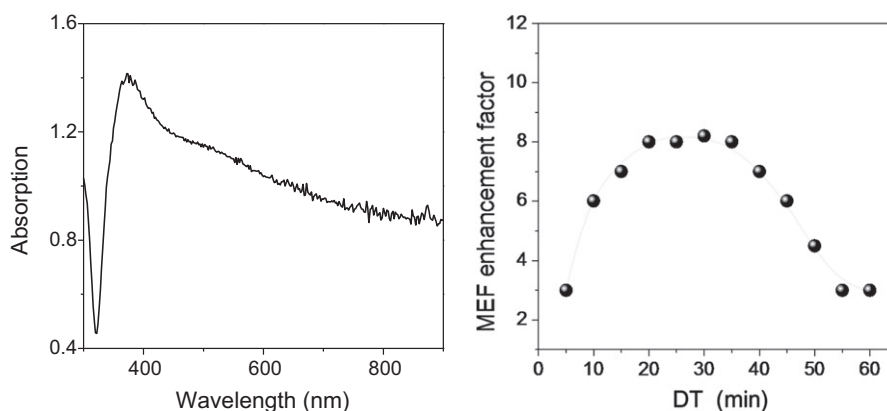


**Fig. 3.** Left: Plasmon resonance absorption band of silver NPs deposited into HBX plate wells (DT = 15 min). Right: Dependence of fluorescein emission on SiF DT. Excitation was at 473 nm using a CW laser line.

along the columns to help understand the role of NP density on enhanced fluorescence. The change in silver DT changes the silver NPs' size and density and subsequently their physical properties on MEF. In particular, it changes the spectral position of the plasmon resonance band, which is a result of the specific change in the absorption and scattering components of plasmon electrons, coupling with the far-field incident light [43]. Fig. 3 shows a characteristic plasmon resonance absorption spectrum of SiFs deposited within Immulon 4 HBX plate wells. The magnitude of the plasmon scattering portion of the extinction spectra increases with the NPs' size and density and shifts to the red [38,43]. Fig. 2 (right panel) clearly demonstrates this physical effect; an increase in silver DT changes the color of the SiFs' reflection from gold–yellow (low DT) to red–gray (greater DT). The color of the SiFs along each row is identical and corresponds to the constant silver DT.

We also characterized the MEF-enhancing property of the SiF wells using standard solutions of fluorescein [43,44]. Fig. 3 (right panel) shows the dependence of the MEF effect (i.e., the ratio of fluorescence intensity measured in the SiF plate well as compared with the intensity of the dye from the original nonsilvered [control] wells). The dependence is nonlinear. The observed MEF effect increases from the onset of deposition, reaching a maximum MEF value of approximately 8 for DT >10 min. A further increase in DT leads to a decline in the MEF enhancement factor. We attribute the decrease in the MEF effect at DT >35 min by the formation of a continuous metal film on the well bottom and the subsequent disappearance of NPs, which are critical for the MEF effect [43].

For assay development, we subsequently used DTs optimized for the maximum MEF effect and to subsequently maximize the fluorescence enhancement of the fluorescein-labeled antibody.

#### *Origin of MEF enhancement of the PA–antibody dye emission and the MEF effect optimization for Immulon 4 HBX SiF plates*

The PA protein effectively binds to the high protein capacity hydrophilic resin that covers the surface of the Immulon 4 HBX plate well bottom. This property of PA can be readily used for its detection using standard ELISA approaches, using horseradish peroxidase (HRP)-based chemiluminescence approaches [45], or (in our case) using a fluorescein-labeled biotin–streptavidin system (i.e., using a fluorescence signal).

To study the effect of silver NPs on the fluorescence signal, we initially used the standard ELISA (see protocol 1 in Materials and Methods) based on a fluorescein-labeled streptavidin–biotin system. Fig. 4 shows the dependence of the fluorescence signal on silver DT. At DT <6 min, the fluorescence signal is low and even decreases slightly with a reduction in DT. An increase at DT >7 min exhibits a sharp rise in fluorescence, which approaches saturation at DT

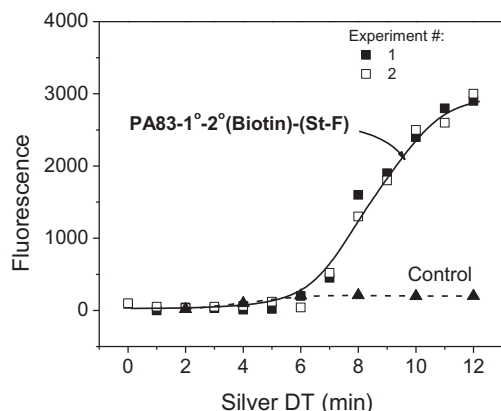
>10 min. Interestingly, the dependences of the MEF effect on silver DT for fluorescein in solution and for that attached to the surface are similar (Fig. 3 [right panel] and Fig. 4), reflecting the generic near-field enhancing properties of MEF. In the case of fluorescein attached to the surface protein complex, the MEF effect shows strong dependence on the silver NPs' size and density, both of which increase on an increase in DT. In addition, the result shows that PA preferentially binds to the hydrophilic resin, which covers the well bottom, but not to the deposited SiFs. In this case, the deposition of NPs decreases the surface area available for PA binding. Subsequently, in the absence of a compensating strong MEF effect, one would expect this to lead to a decrease in the signal. To understand this change in MEF, which is known to depend strongly on near-field (electric field) distribution and intensity, we performed theoretical FDTD simulations of the system.

Fig. 5 shows the results of FDTD simulations of the near field for the progressive change of SiFs' density on a glass surface, a model system for our wells. At large interparticle distance (low SiFs' density), the near-field intensity around NPs is low at approximately 20 a.u. (note that incident far-field intensity is an arbitrary 1.0). The intensity increases nearly 10-fold (the intensity of the near-field at  $D = 10$  nm is  $\sim 200$  a.u.) on a decrease in the interparticle distance. A remarkable localized enhancement of the electric near field is a result of the resonance interaction between the plasmon systems of two adjacent silver NPs. The change in the near-field intensity is nonlinear, is observed only on quite short interparticle distances (<30 nm), and correlates well with the fluorescence enhancement shown in Fig. 4. In this case, the total enhancement of fluorescence could be considered as a superposition of at least two effects, enhanced absorption and enhanced emission: coupling of a dye with NP surface plasmons (i.e., resonance interaction between electronic systems of a chromophore and an NP) (enhanced emission) and the enhanced intensity of the near field between the NPs (i.e., the field that forms the spacial distribution of high-frequency energy in the interparticle space that interacts with oscillating electronic system of proximal chromophores [38]) (enhanced absorption). It should be noted that the role of the near-field intensity and spacial distribution (volume) in the MEF effect was recently theoretically postulated and experimentally verified by our laboratory [44].

Based on these optimized surface properties for MEF, we subsequently proposed an MEF–PA assay system that is optimized for MEF (Fig. 6).

#### *MEF of the PA–antibody–fluorescein system observed in SiF well plates*

To characterize the magnitude of the MEF effect in SiF well plates for the MEF–PA assay, we compared fluorescence signals



**Fig. 4.** Fluorescence of the chromophore (fluorescein), attached to the multiprotein complex within SiF wells, nonlinearly depends on silver DT. Loading of the PA protein and its detection, using primary (1°) and secondary (2°) biotinylated antibody and fluorescein-labeled streptavidin, was undertaken using an ELISA-like protocol (see protocol 1 in Materials and Methods). Control: streptavidin–fluorescein incubated for 10 min in SiF plate wells. Fluorescence excitation was undertaken using a 473-nm laser line, and emission was collected at 520 nm.

from SiF plates and control plates (i.e., plates containing no silver). Fig. 7 shows the MEF effect calculated as the ratio of the fluorescence signal of the fluorescein-labeled PA–antibody complex formed in SiF plates to the fluorescence signal from the control samples prepared in original nonsilvered Immulon plates. A decrease in the enhancement factor at larger loading concentrations of PA, >1 nM (>80 µg/ml), was evident and could be explained by self-quenching of the fluorophores due to fluorescence resonant energy transfer (homo-FRET) between identical labels. Homo-FRET increases with a decrease in the distance between fluorophores

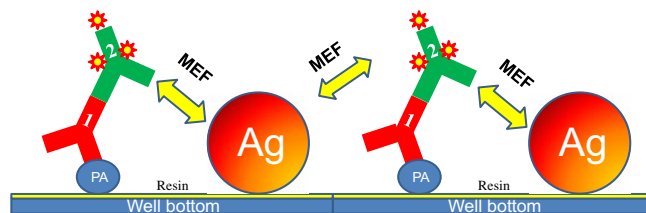


**Fig. 6.** Geometrical scheme of the MEF–PA assay. The multiprotein complex (PA, primary antibody, and secondary antibody labeled with fluorescein) is attached to the Immulon 4 HBX plate bottom resin. The MEF of fluorescein is induced by close proximity to the silver NPs deposited within wells and also depends on the size and density of SiFs.

and, subsequently, with an increase in protein density on the surface.

The magnitude of the MEF effect for the limited range of loaded PA concentrations is approximately 20. This value of the MEF effect reflects the ratio of intensities measured from the surfaces (sample and control) of equal area (i.e., reflects not only the “real” MEF effect but also the difference in the amount of the labeled protein complexes attached to the surface). At silver DT = 10 to 15 min, the approximate OD of SiF wells at 473 nm (wavelength of excitation) is 1.0 to 1.3. If we assume that the cross section of NP absorption is close to the NPs’ size (diameter), one can estimate the fraction of NPs’ free area as  $f_{\text{free}} = 10^{-\text{OD}}$ , which is approximately 5 to 10% of the total surface area. As we have shown, the PA protein binds preferentially to the hydrophilic surface of the well resin, and one can suggest that the amount of PA attached to the SiF surface is 10- to 20-fold less as compared with the nonsilvered surface. In that case, we can correct the observed MEF value, which would correspond to an equal amount of dye-labeled complex on the

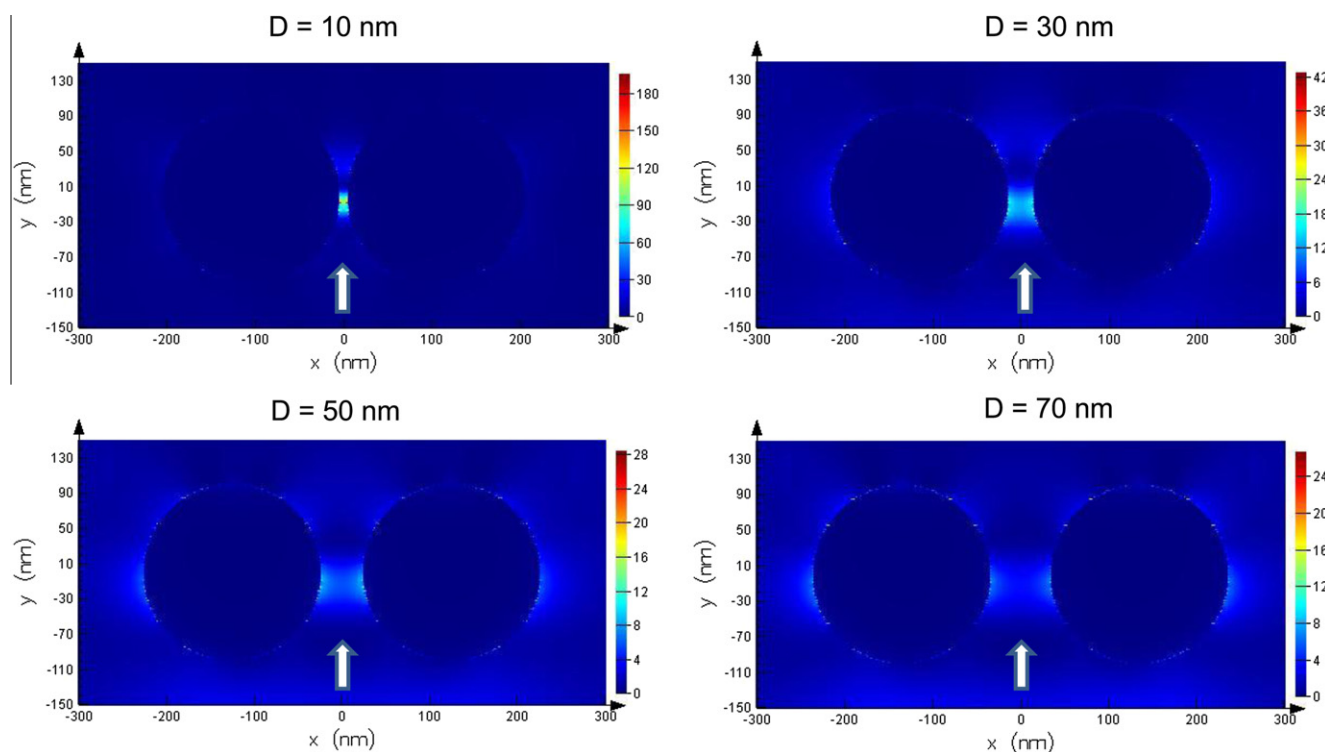


**Fig. 5.** FDTD simulations of the near field for the progressive change of SiF NPs’ density (radius = 100 nm). Two NPs are attached to the glass slide (a glass slide is on the top of the NPs); the white arrow shows the direction of the incident light (473 nm). The intensity of the near field increases from approximately 20 to 200 a.u. on a decrease in the interparticle distance ( $D$ ).  $D$  is the distance between the surfaces of two silver NPs that changes on SiF DT.

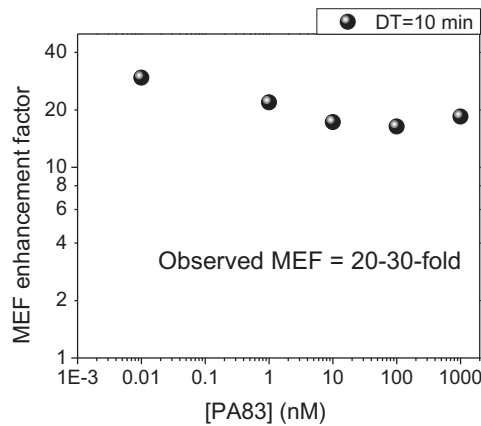


**Fig. 7.** MEF effect observed for different loading concentrations of PA. MEF was measured as a ratio of the fluorescence intensity of the fluorescein-labeled PA antibody complex and measured in SiF plates to the observed fluorescence intensity from the control samples, that is, in original Immulon plates (no SiFs). Silver DT = 10 min.

surface. Subsequently, we estimate an enhancement factor in the range of 200- to 400-fold.

#### Characterization of the ultra-sensitive rapid MEF-PA assay

Fig. 8 demonstrates the kinetics of PA attachment to the Immulon plate wells covered with silver NPs. The incubation time of PA changed from 5 to 40 min, followed by washing the wells and then proceeding to follow protocol 2 (see Materials and Methods). The dependence of the fluorescence signal on incubation time shows that the attachment of PA to well bottoms approaches saturation at an incubation time longer than 20 min.

Microwave irradiation (MW) of the plates filled with the PA solution significantly accelerates the protein absorption to the surface. Fig. 9 shows the kinetics of microwave-accelerated attachment of PA to the SiF wells. Measurements were undertaken at the same conditions as undertaken without MW, as shown in Fig. 8. The magnitude of the fluorescence signal collected from the wells reaches the same saturated value ( $F = 6500$  a.u.) but in 20 to 30 s (i.e., the process is accelerated ~60-fold as compared with non-MW conditions).

The flow diagram for the rapid MEF-PA assay protocol is shown in Fig. 10. The total time of the assay, including microwave-accelerated absorption of PA on the surface, is less than 40 min. Using

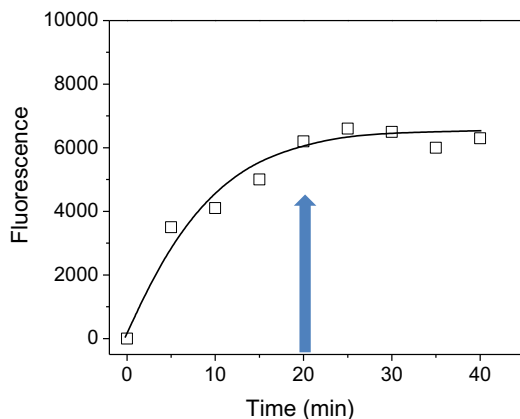


**Fig. 8.** Room temperature kinetics of PA attachment to the SiF well Immulon plate surface.

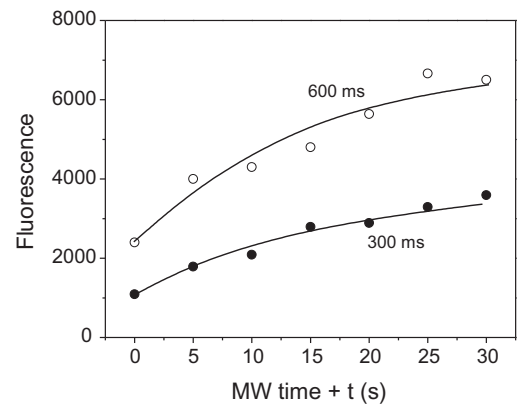


**Fig. 9.** Kinetics of the microwave-accelerated attachment of the PA protein to the plate well bottom. Microwave irradiation of PA in milk (milk/water = 1:20), loaded onto SiF wells (Immulon), was undertaken for different irradiation times followed by treatment with blocking solution and antibodies ( $1^\circ$  and  $2^\circ$ -FITC). The fluorescence intensity was measured at two integration times: 300 and 600 ms. The lag time ( $t$ ) between irradiation and fluorescence measurement was 1 to 2 min. The fluorescence signal from wells without PA was negligible.

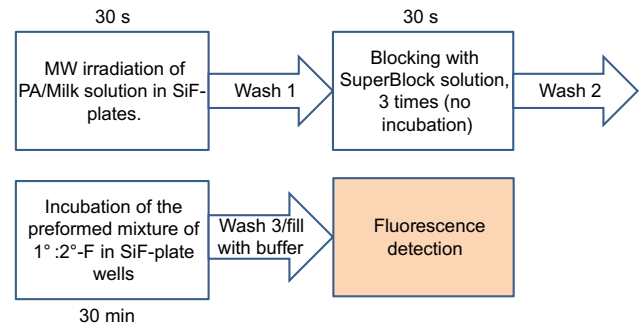


**Fig. 10.** Flow diagram of MEF-PA assay sequential procedures.  $2^\circ$ -F, secondary antibody labeled with fluorescein.

this protocol, we measured the MEF-PA assay sensitivity in the SiF plates using different loading concentrations of PA (from 10 ng/ml to 0.01 pg/ml) and the control (no PA in the samples) (Fig. 11). The MEF-PA assay demonstrates extremely high sensitivity to PA—approaching the pg/ml level. Fluorescence readings from the plates can be reliably registered, even for the PA loading con-

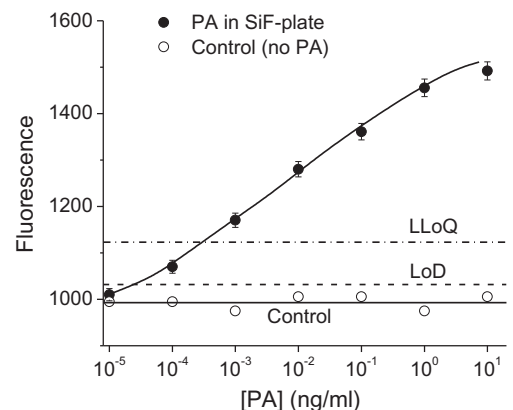


**Fig. 11.** PA assay sensitivity curves measured in SiF plates. Fluorescence for the PA samples and control (no PA) was measured in SiF plates. LoD = mean fluorescence +  $3 \times$  standard deviation (dashed line); LLoQ =  $10 \times$  standard deviation (dashed-dotted line).

centration of 0.1 pg/ml. We calculated the limit of detection (LoD) and lower limit of quantitation (LLOQ) for PA; the LoD is 0.1 pg/ml, and the LLOQ is 1 pg/ml. Taking into account that the loading volume of the PA solution (1 pg/ml) is 80  $\mu$ l, one can estimate the number of protein molecules in one well as  $n = N_A \times [\text{PA}] \times V = 10^6$ , where  $N_A$  is Avagadro's number. Consequently, the MEF-PA assay is sensitive to approximately 1 million PA molecules in our SiF plate well. This suggests that, as shown in Fig. 11, our analytical sensitivity is better than 1 pg/ml.

## Conclusions

In this article, we have described an ultra-sensitive and rapid MEF-PA assay based on both enhancement of the fluorescence signal by silver NPs (SiFs) and microwave-accelerated absorption of a protein onto a surface. Our designed "rapid catch and signal" (RCS) technology for the PA protein can potentially be used for other protein antigens, as well as toxins, by simply changing the capture antibody. Our approach allows the possibility of detecting PA at high sensitivity in less than 40 min.

## Acknowledgments

The authors thank the Biological Defense Research Directorate, Naval Medical Research Center, for financial support (work unit number 00000123002) and are grateful for the financial support of the Institute of Fluorescence (IoF) at the University of Maryland, Baltimore County. The authors also acknowledge the support and discussions of Les Baillie (Cardiff University, UK). The views expressed in this article are those of the authors and do not necessarily reflect the official policy or position of the Department of the Navy, Department of Defense, or US government.

## References

- [1] R. Frank, R. Hargreaves, Clinical biomarkers in drug discovery and development, *Nat. Rev. Drug Discovery* 2 (2003) 566–580.
- [2] P.C. Turnbull, Introduction: anthrax history, disease, and ecology, *Curr. Top. Microbiol. Immunol.* 271 (2002) 1–19.
- [3] K.A. Edwards, H.A. Clancy, A.J. Baeumner, *Bacillus anthracis*: toxicology, epidemiology, and current rapid-detection methods, *Anal. Bioanal. Chem.* 384 (2006) 73–84.
- [4] P.S. Brachman, Inhalation anthrax, *Ann. N.Y. Acad. Sci.* 353 (1980) 83–93.
- [5] J.A. Jernigan, D.S. Stephens, D.A. Ashford, C. Omenaca, M.S. Topiel, M. Galbraith, M. Tapper, T.L. Fisk, S. Zaki, T. Popovic, R.F. Meyer, C.P. Quinn, S.A. Harper, S.K. Fridkin, J.J. Sejvar, C.W. Shepard, M. McConnell, J. Guarner, W.J. Shieh, J.M. Malecki, J.L. Gerberding, J.M. Hughes, B.A. Perkins, Bioterrorism-related inhalational anthrax: the first 10 cases reported in the United States, *Emerg. Infect. Dis.* 7 (2001) 933–944.
- [6] H. Smith, J. Keppie, Observations on experimental anthrax: demonstration of a specific lethal factor produced in vivo by *Bacillus anthracis*, *Nature* 173 (1954) 869–870.
- [7] H. Smith, J. Keppie, J.L. Stanley, P.W. Harris-Smith, The chemical basis of the virulence of *Bacillus anthracis*: IV. Secondary shock as the major factor in death of guinea pigs from anthrax, *Br. J. Exp. Pathol.* 36 (1955) 323–335.
- [8] T.C. Dixon, M. Meselson, J. Guillemin, P.C. Hanna, Anthrax, *N. Engl. J. Med.* 341 (1999) 815–826.
- [9] D.R. Franz, P.B. Jahrling, A.M. Friedlander, D.J. McClain, D.L. Hoover, W.R. Bryne, J.A. Pavlin, G.W. Christopher, E.M. Eitzen Jr., Clinical recognition and management of patients exposed to biological warfare agents, *JAMA* 278 (1997) 399–411.
- [10] K.C. Brittingham, G. Ruthel, R.G. Panchal, C.L. Fuller, W.J. Ribot, T.A. Hoover, H.A. Young, A.O. Anderson, S. Bavari, Dendritic cells endocytose *Bacillus anthracis* spores: implications for anthrax pathogenesis, *J. Immunol.* 174 (2005) 5545–5552.
- [11] A. Cleret, A. Quesnel-Hellmann, A. Vallon-Eberhard, B. Verrier, S. Jung, D. Vidal, J. Mathieu, J.N. Tournier, Lung dendritic cells rapidly mediate anthrax spore entry through the pulmonary route, *J. Immunol.* 178 (2007) 7994–8001.
- [12] C. Guidi-Rontani, M. Levy, H. Ohayon, M. Mock, Fate of germinated *Bacillus anthracis* spores in primary murine macrophages, *Mol. Microbiol.* 42 (2001) 931–938.
- [13] J.M. Ross, The pathogenesis of anthrax following the administration of spores by the respiratory route, *J. Pathol. Bacteriol.* 73 (1957) 485–494.
- [14] J. Stephen, Anthrax toxin, in: F. Dornier, J. Drews (Eds.), *Pharmacology of Bacterial Toxins*, Pergamon, Oxford, UK, 1986, pp. 381–395.
- [15] K.R. Klimpel, S.S. Molloy, G. Thomas, S.H. Leppla, Anthrax toxin protective antigen is activated by a cell surface protease with the sequence specificity and catalytic properties of furin, *Proc. Natl. Acad. Sci. USA* 89 (1992) 10277–10281.
- [16] J. Mogridge, K. Cunningham, R.J. Collier, Stoichiometry of anthrax toxin complexes, *Biochemistry* 41 (2002) 1079–1082.
- [17] J. Mogridge, K. Cunningham, D.B. Lacy, M. Mourez, R.J. Collier, The lethal and edema factors of anthrax toxin bind only to oligomeric forms of the protective antigen, *Proc. Natl. Acad. Sci. USA* 99 (2002) 7045–7048.
- [18] P.S. Brachman, A. Kaufman, *Bacterial Infections of Humans: Epidemiology and Control*, Plenum Medical, New York, 1998.
- [19] J.C. Milne, D. Furlong, P.C. Hanna, J.S. Wall, R.J. Collier, Anthrax protective antigen forms oligomers during intoxication of mammalian cells, *J. Biol. Chem.* 269 (1994) 20607–20612.
- [20] B.E. Turk, Manipulation of host signalling pathways by anthrax toxins, *Biochem. J.* 402 (2007) 405–417.
- [21] M.N. Swartz, Recognition and management of anthrax—an update, *N. Engl. J. Med.* 345 (2001) 1621–1626.
- [22] E.R. Swanson, D.E. Fosnocht, Anthrax threats: a report of two incidents from Salt Lake City, *J. Emerg. Med.* 18 (2000) 229–232.
- [23] J.J. Walsh, N. Pesik, C.P. Quinn, V. Urdaneta, C.A. Dykewicz, A.E. Boyer, J. Guarner, P. Wilkins, K.J. Norville, J.R. Barr, S.R. Zaki, J.B. Patel, S.P. Reagan, J.L. Pirkle, T.A. Treadwell, N.R. Messonnier, L.D. Rotz, R.F. Meyer, D.S. Stephens, A case of naturally acquired inhalation anthrax: clinical care and analyses of anti-protective antigen immunoglobulin G and lethal factor, *Clin. Infect. Dis.* 44 (2007) 968–971.
- [24] D. Kobiler, S. Weiss, H. Levy, M. Fisher, A. Mechaly, A. Pass, Z. Altboum, Protective antigen as a correlative marker for anthrax in animal models, *Infect. Immun.* 74 (2006) 5871–5876.
- [25] R. Mabry, K. Brasky, R. Geiger, R. Carrion Jr., G.B. Hubbard, S. Leppla, J.L. Patterson, G. Georgiou, B.L. Iverson, Detection of anthrax toxin in the serum of animals infected with *Bacillus anthracis* by using engineered immunoassays, *Clin. Vaccine Immunol.* 13 (2006) 671–677.
- [26] S. Tang, M. Moayeri, Z. Chen, H. Harma, J. Zhao, H. Hu, R.H. Purcell, S.H. Leppla, I.K. Hewlett, Detection of anthrax toxin by an ultrasensitive immunoassay using europium nanoparticles, *Clin. Vaccine Immunol.* 16 (2009) 408–413.
- [27] M. Moayeri, J.F. Wiggins, S.H. Leppla, Anthrax protective antigen cleavage and clearance from the blood of mice and rats, *Infect. Immun.* 75 (2007) 5175–5184.
- [28] R.E. Biagini, D.L. Sammons, J.P. Smith, E.H. Page, J.E. Snawder, C.A. Striley, B.A. MacKenzie, Determination of serum IgG antibodies to *Bacillus anthracis* protective antigen in environmental sampling workers using a fluorescence covalent microsphere immunoassay, *Occup. Environ. Med.* 61 (2004) 703–708.
- [29] R.T. Cummings, S.P. Salowe, B.R. Cunningham, J. Wiltsie, Y.W. Park, L.M. Sonatore, D. Wisniewski, C.M. Douglas, J.D. Hermes, E.M. Scolnick, A peptide-based fluorescence resonance energy transfer assay for *Bacillus anthracis* lethal factor protease, *Proc. Natl. Acad. Sci. USA* 99 (2002) 6603–6606.
- [30] T.N. Huan, T. Ganesh, S.H. Han, M.Y. Yoon, H. Chung, Sensitive detection of an anthrax biomarker using a glassy carbon electrode with a consecutively immobilized layer of polyaniline/carbon nanotube/peptide, *Biosens. Bioelectron.* 26 (2011) 4227–4230.
- [31] A.E. Boyer, M. Gallegos-Candela, R.C. Lins, Z. Kuklenyik, A. Woolfitt, H. Moura, S. Kalb, C.P. Quinn, J.R. Barr, Quantitative mass spectrometry for bacterial protein toxins: a sensitive, specific, high-throughput tool for detection and diagnosis, *Molecules* 16 (2011) 2391–2413.
- [32] K. Aslan, I. Gryczynski, J. Malicka, E. Matveeva, J.R. Lakowicz, C.D. Geddes, Metal-enhanced fluorescence. An emerging tool in biotechnology, *Curr. Opin. Biotechnol.* 16 (2005) 55–62.
- [33] K. Aslan, C.D. Geddes, Microwave-accelerated metal-enhanced fluorescence. Platform technology for ultrafast and ultrabright assays, *Anal. Chem.* 77 (2005) 8057–8067.
- [34] K. Aslan, C.D. Geddes, New tools for rapid clinical and bioagent diagnostics: microwaves and plasmonic nanostructures, *Analyst* 133 (2008) 1469–1480.
- [35] K. Aslan, J. Huang, G.M. Wilson, C.D. Geddes, Metal-enhanced fluorescence-based RNA sensing, *J. Am. Chem. Soc.* 128 (2006) 4206–4207.
- [36] K. Aslan, Y.X. Zhang, S. Hibbs, L. Baillie, M.J.R. Previte, C.D. Geddes, Microwave-accelerated metal-enhanced fluorescence. Application to detection of genomic and exosporium anthrax DNA in <30 s, *Analyst* 132 (2007) 1130–1138.
- [37] A.I. Dragan, K. Golberg, A. Elbaz, R. Marks, Y. Zhang, C.D. Geddes, Two-color, 30-second microwave-accelerated metal-enhanced fluorescence DNA assays: a new rapid catch and signal (RCS) technology, *J. Immunol. Methods* 366 (2010) 1–7.
- [38] C.D. Geddes (Ed.), *Metal-Enhanced Fluorescence*, John Wiley, Hoboken, NJ, 2010.
- [39] C.D. Geddes, J.R. Lakowicz, Metal-enhanced fluorescence, *J. Fluoresc.* 12 (2002) 121–129.
- [40] K. Aslan, P. Holley, C.D. Geddes, Microwave-accelerated metal-enhanced fluorescence (MAMEF) with silver colloids in 96-well plates: application to ultra fast and sensitive immunoassays, high throughput screening, and drug discovery, *J. Immunol. Methods* 312 (2006) 137–147.
- [41] K. Aslan, C.D. Geddes, Microwave-accelerated metal-enhanced fluorescence (MAMEF): application to ultra fast and sensitive clinical assays, *J. Fluoresc.* 16 (2006) 3–8.
- [42] M.T. Albrecht, H. Li, E.D. Williamson, C.S. LeButt, H.C. Flick-Smith, C.P. Quinn, H. Westra, D. Galloway, A. Mateczun, S. Goldman, H. Groen, L.W. Baillie, Human monoclonal antibodies against anthrax lethal factor and protective

- antigen act independently to protect against *Bacillus anthracis* infection and enhance endogenous immunity to anthrax, *Infect. Immun.* 75 (2007) 5425–5433.
- [43] R. Pribik, A.I. Dragan, Y. Zhang, C. Gaydos, C.D. Geddes, Metal-enhanced fluorescence (MEF): physical characterization of silver island films and exploring sample geometries, *Chem. Phys. Lett.* 478 (2009) 70–74.
- [44] A.I. Dragan, C.D. Geddes, Excitation volumetric effects (EVE) in metal-enhanced fluorescence, *Phys. Chem. Chem. Phys.* 13 (2011) 3831–3838.
- [45] R.P. Huang, Detection of multiple proteins in an antibody-based protein microarray system, *J. Immunol. Methods* 255 (2001) 1–13.